optica

Observation of Poynting's vector reversal in an active photonic cavity

Ali K. Jahromi and Ayman F. Abouraddy*

CREOL, The College of Optics & Photonics, University of Central Florida, Orlando, Florida 32816, USA
**Corresponding author: raddy@creol.ucf.edu*

Received 15 April 2016; revised 17 June 2016; accepted 28 June 2016 (Doc. ID 263319); published 24 October 2016

Optical power flow along an active cavity having net gain can differ dramatically from that in a passive cavity. We report the first observation of Poynting's vector reversal in an active cavity under scattering boundary conditions. At a sub-lasing gain, which we call Poynting's threshold, a null develops in Poynting's vector, which divides the cavity into sections with oppositely directed energy flows. Furthermore, we demonstrate that the direction of Poynting's vector at a fixed point in an active cavity can be controllably reversed without changing its magnitude via an intra-cavity passive element, thereby suggesting a potential methodology for optical switching.

OCIS codes: (050.2230) Fabry-Perot; (260.3160) Interference; (140.3410) Laser resonators.

http://dx.doi.org/10.1364/OPTICA.3.001194

1. INTRODUCTION

Optical gain is the key enabler for the operation of lasers and laser amplifiers [1,2] and thus underlies many modern amenities of everyday life [3]. The investigation of optical gain has a long history, dating back to Einstein's introduction of this concept in the context of stimulated emission [4]. Since then, the propagation of light in media featuring *resonant* gain, in particular, has been the focus of many fundamental studies, ultimately leading to the concept of "fast light," which is a consequence of pulse reshaping on resonance [5–10]. These dispersive effects have been observed in a variety of optical platforms, including coherent population oscillations in crystals [11] and quantum wells [12], in quantum dot semiconductor optical amplifiers via population oscillation [13–15], stimulated Brilluoin gain in non-linear fibers [16], and erbium-doped fibers [17].

More recently, non-Hermitian optical systems with a spatially engineered distribution of optical gain and loss are now being actively explored to exploit the rich physics of exceptional points [18] and spectral singularities [19], among other phenomena associated with non-Hermitian structures [20]. In particular, parity and time-reversal (PT)-symmetric systems [21–23] may yield nonmagnetic isolators [24] and offer useful control over lasing action [25,26]. Moreover, the role of gain in compensating for inevitable losses in plasmonic systems has prompted investigations of the interplay between the amplification and field concentration [27,28]. It is therefore imperative to appreciate the subtleties involved in these non-Hermitian configurations where optical gain, which is usually far from resonance, interacts with confined fields in conjunction with coherent feedback provided by reflections at interfaces, coupling across barriers, or circulation in ring resonators. Indeed, the interplay between gain and feedback in a cavity can lead to a host of phenomena that are still not fully appreciated [29–32] and raises fundamental questions regarding causality [33–36]. A large number of theoretical studies have focused on this question, but experimental investigations are lacking.

In this paper, we examine the distribution of Poynting's vector [37] within an active optical cavity at sub-lasing gain values under *scattering boundary conditions*; that is, with an optical probe externally incident on the cavity from one port. Scattering boundary conditions enforce a constraint: Poynting's vector $\vec{\mathcal{P}}$ at the cavity exit is necessarily directed forward in the same direction of the probe, a condition that applies whether the cavity is passive (lossy) or active (has net single-pass gain), and whether the probe is on- or off-resonance. As a consequence of this constraint, when the net gain in a planar cavity reaches a critical value that we term "Poynting's threshold," $\vec{\mathcal{P}}$ is *extinguished* at the cavity entrance. The location of this null in $\vec{\mathcal{P}}$, and hence a null in the net power flow, migrates into the cavity upon further increase of the gain. The null plane of $\vec{\mathcal{P}}$ divides the cavity into two sections: in the vicinity of the exit, $\vec{\mathcal{P}}$ points *forward*, while $\vec{\mathcal{P}}$ reverses direction and points *backward*, opposing the probe, in the vicinity of the cavity entrance. At Poynting's threshold, the linear response of the system produces a backward-propagating signal with equal intensity to the probe as well as an amplified forward-propagating signal. Thus, this threshold corresponds to *unity reflectivity* of the total system, where there is no net flux through the boundary of the cavity at any wavelength within the gain bandwidth, both on- and off-resonance. Despite a large number of theoretical studies that have tackled this active-cavity configuration from the perspective of causality (see Refs. 30,35 for a review of the literature), there have been, to the best of our knowledge, no experimental investigation of these predictions.

In contrast to fast-light effects, the phenomena we examine here are *not* a consequence of a resonance in the gain spectrum, as we confirm by exploiting broadband (40 nm) semiconductor optical amplifiers (SOAs) and a continuous wave probe. To *unambiguously* determine the direction of $\vec{\mathcal{P}}$ within the cavity, we construct a single-mode fiber-based polarization-maintaining cavity in which the forward and backward paths are isolated via in-line polarization components. This configuration, furthermore, helps avoid any effects of spatial-hole burning. By increasing the net gain in the cavity, we identify the transition from an all-forward regime for $\vec{\mathcal{P}}$ to a regime where the energy flow is segmented into forward- and backward-pointing $\vec{\mathcal{P}}$ sections separated by a null in $\vec{\mathcal{P}}$ once Poynting's threshold is exceeded. Since the cavity net gain determines Poynting's threshold, a *tunable* passive intra-cavity element in addition to a *fixed* gain element can be exploited to controllably reverse the direction of $\vec{\mathcal{P}}$ in the cavity. This concept suggests a potential methodology for optical switching in non-Hermitian photonic systems.

2. ACTIVE-CAVITY MODEL

We first introduce a simple one-dimensional active-cavity model that captures the relevant physics. Consider the planar cavity shown in Fig. 1 consisting of two lossless mirrors M_1 and M_2 (reflectivities R_1 and R_2, respectively) sandwiching a layer of thickness L and complex refractive index $n = n_r + in_i$; here, the positive (negative) sign of n_i corresponds to loss (gain). We assume scattering boundary conditions, whereupon a scalar probe is incident normally on the cavity from the left and there is no incoming wave from the right.

Solving Maxwell's equation in the active cavity subject to these boundary conditions yields forward $E_f(z)$ and backward $E_b(z)$ field distributions for monochromatic waves along the cavity axis z, and corresponding intensities $I_f(z)$ and $I_b(z)$, respectively, with $I_f(z)$ given by

$$I_f(z) = \frac{(1-R_1)G(z)}{1 + R_1R_2G^2 - 2\sqrt{R_1R_2}G\cos\varphi}; \tag{1}$$

here, φ is the cavity round-trip phase; $G \geq 1$ is the single-pass cavity gain; $G(z) = e^{gz}$ is the gain after traversing a distance z from M_1, where $g = 2|n_i|k$ and k is the wave number, such that $G(0) = 1$ and $G(L) = G$; and $I_f(z)$ is normalized such that the incident intensity is unity (see Supplement 1 for a detailed transfer-matrix formulation of this cavity model). In contrast to studies of fast light in *resonant* gain media, we consider here a broad gain bandwidth with constant G. If gain is replaced by loss, then the cavity single-pass gain $G > 1$ in Eq. (1) is simply replaced by the cavity single-pass loss $\mathcal{L} < 1$. The intensity of the forward and backward propagating waves are related (Supplement 1) via

$$\frac{I_f(z)}{I_b(z)} = \frac{1}{R_2}\left(\frac{G(z)}{G}\right)^2. \tag{2}$$

Critically, this relationship is independent of φ and thus applies on *and* off the cavity resonances. Poynting's vector $\vec{\mathcal{P}}(z) = \frac{1}{2}\Re\{\vec{E}\times\vec{H}^*\} = \mathcal{P}_z\hat{z}$ has a single axial component,

$$\mathcal{P}_z(z) = \frac{n_r}{2\eta_o}\{|E_f(z)|^2 - |E_b(z)|^2\} + \frac{n_i}{\eta_o}\Im\{E_f(z)E_b^*(z)\} \tag{3}$$

$$\approx I_f(z) - I_b(z), \tag{4}$$

where $\Re\{\cdot\}$ and $\Im\{\cdot\}$ indicate the real and imaginary parts, respectively, and η_o is the free-space electromagnetic impedance. The second term on the right-hand side of Eq. (3) is usually neglected, although it can have significant impact in some cases; see Ref. [38]. In our experiment, this interference term is negligible with respect to the first term in Eq. (3), as we confirm below [30]. Therefore, $\vec{\mathcal{P}}$ points forward ($\mathcal{P}_z > 0$) in the direction of the incident wave whenever $I_f(z) > I_b(z)$, and points backward towards the source otherwise, $I_f(z) < I_b(z) \rightarrow \mathcal{P}_z < 0$.

Scattering boundary conditions enforce a constraint on the forward and backward waves at the cavity exit: $I_f(L)/I_b(L) = 1/R_2 \geq 1$. In addition to applying on- and off-resonance, this condition applies to active and passive cavities; in all cases, $I_f(L) \geq I_b(L)$, and $\vec{\mathcal{P}}$ consequently always points forward at the cavity exit. This constraint serves to anchor the problem and dictates the direction of $\vec{\mathcal{P}}$ within the cavity by back propagating the fields from $z = L$. At the cavity entrance $z = 0$, on the other hand, we have $I_f(0)/I_b(0) = 1/(R_2G^2)$, a ratio that may be larger *or* smaller than unity. If $I_f(0) > I_b(0)$, $\vec{\mathcal{P}}$ points forward, which applies to passive and low-gain cavities, when $I_f(0) < I_b(0)$, $\vec{\mathcal{P}}$ reverses direction and points backward towards the source. Of

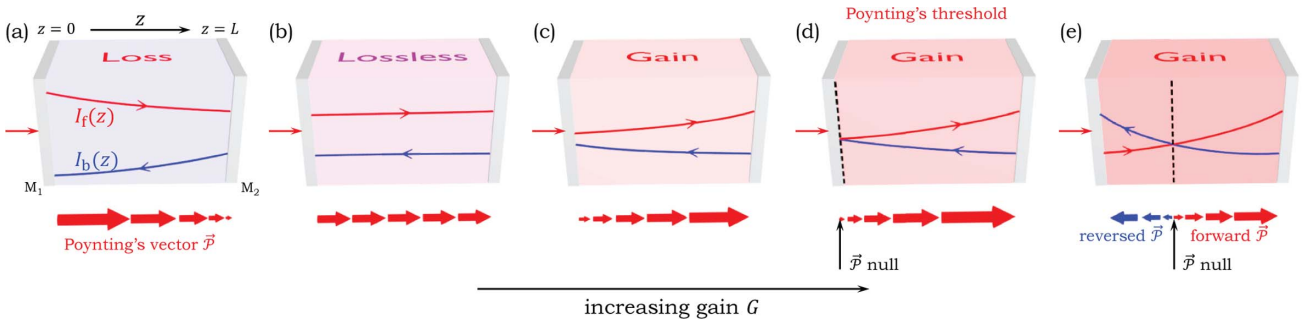

Fig. 1. Concept of Poynting's vector reversal in an active planar photonic cavity defined by mirrors M_1 and M_2 having reflectivities R_1 and R_2, respectively. The cavity forward $I_f(z)$ and backward $I_b(z)$ waves are depicted in red and blue, respectively, and the large arrows below the cavity correspond to Poynting's vector $\vec{\mathcal{P}}(z)$. The size of the arrow corresponds to the amplitude of $\vec{\mathcal{P}}(z)$. (a) In a *lossy* cavity, $I_f(z)$ and $I_b(z)$ decay, and $\vec{\mathcal{P}}$ points in the forward direction everywhere. At the cavity exit $z = L$, $I_b(L)/I_f(L) = R_2 < 1$, where R_2 is the reflectivity of M_2. (b) In a *passive* cavity (no gain or loss), $I_f(z)$ and $I_b(z)$ are constant along z, with $I_b(z) < I_f(z)$, and $\vec{\mathcal{P}}$ points in the forward direction everywhere. (c) In an *active* cavity, I_f and I_b grow in reversed directions with respect to the lossy cavity in (a); $\vec{\mathcal{P}}$ still points in the forward direction everywhere. (d) By increasing gain to Poynting's threshold $G = G_P = 1/\sqrt{R_2}$, a null develops in the power flow at the entrance $\vec{\mathcal{P}}(0) = 0$. (e) Increasing $G > G_P$, the null in G_P moves within the cavity, which is now split into two sections, with $\vec{\mathcal{P}}$ reversing its direction such that it points toward the source in the section closer to the cavity entrance.

particular interest is the transition threshold $I_f(0) = I_b(0)$ between these two regimes, whereupon $\vec{\mathcal{P}}$ is extinguished at $z = 0$. This critical gain value, which we call "Poynting's threshold," corresponds to a cavity single-pass gain of $G_P = 1/\sqrt{R_2}$. Note that Poynting's threshold always precedes the lasing threshold $G_L = 1/\sqrt{R_1 R_2} > G_P$; that is, G_P is always a sub-lasing gain value.

We are now in a position to examine the dynamics of $\vec{\mathcal{P}}$ along a cavity, starting from a lossy condition and gradually compensating for the loss until the cavity has net gain; five instances are depicted in Figs. 1(a)–1(e). Starting from $I_f(L) > I_b(L)$ at the exit of a lossy cavity ($n_i > 0$), we back propagate the forward and backward waves to the entrance [see Fig. 1(a)]. Here, $I_f(z) > I_b(z)$, and $\vec{\mathcal{P}}$ points forward everywhere, but its amplitude decays with z. In a lossless cavity ($n_i = 0$), $\vec{\mathcal{P}}$ again points forward everywhere, but its amplitude is independent of z [see Fig. 1(b)].

The situation changes once the cavity becomes active ($n_i < 0$) [Figs. 1(c)–1(e)]. Here, the growth directions for $I_f(z)$ and $I_b(z)$ are in opposition to those in the passive case. For values of $G < G_P$, $\vec{\mathcal{P}}$ still points forward everywhere, but its amplitude now *grows* with z [see Fig. 1(c)]. When Poynting's threshold is reached, $G = G_P$, we have $I_f(0) = I_b(0)$, and a null develops in $\vec{\mathcal{P}}$ at the entrance, $\vec{\mathcal{P}}(0) = 0$ [see Fig. 1(d)]; $\vec{\mathcal{P}}(z)$ points forward otherwise. When $G > G_P$, a new situation arises. For the first time, $I_f(0) < I_b(0)$ [Fig. 1(e)], and the null in $\vec{\mathcal{P}}$ moves to $z = z_P = L\{1 - \ln G_P / \ln G\}$ and the cavity divides into two segments: in the region $0 < z < z_P$, $\vec{\mathcal{P}}$ points *backwards* towards the source in opposition to the probe; in the region $z_P < z < L$, $\vec{\mathcal{P}}$ points *forwards*, in the same direction as the probe. Finally, when G reaches the lasing threshold $G = G_L$, lasing is initiated and the null in $\vec{\mathcal{P}}$ reaches the cavity midpoint $z = z_P = L/2$ in a symmetric cavity ($R_1 = R_2$). Once lasing commences, the cavity becomes a nonlinear system and a different analysis is required, which we do not pursue here. We proceed to describe the experimental arrangement we have constructed to confirm these predictions.

3. EXPERIMENT

One of the critical desiderata to facilitate the observation of the reversal of $\vec{\mathcal{P}}$ when $G > G_P$ is that the cavity allows for probing the forward and backward waves independently. We make use of a single-mode fiber-based cavity in which we separate the forward and backward paths by means of optical isolators, in-line polarizers, and polarization controllers, while the gain is provided by broadband SOAs [see Fig. 2(a)]. This arrangement provides a one-dimensional implementation that eliminates spurious spatial-mode or polarization effects; it allows tuning all the cavity degrees of freedom independently, and fiber couplers are inserted at any location in the cavity to probe the power (see Supplement 1 for further details). We emphasize that the forward and backward paths are spatially separated here as a matter of convenience to unambiguously determine the direction of $\vec{\mathcal{P}}$ (the blue and red paths in Fig. 2), but they may of course be combined (the black paths in Fig. 2).

The cavity is defined by symmetric fiber mirrors $R_1 = R_2 = R = 0.5$ [see Fig. 2(b)]. The SOAs provide broadband optical gain over a 40 nm bandwidth [see Fig. 2(c)], and the probe is a tunable continuous wave laser centered at a wavelength ≈1551.5 nm with a linewidth full width at half-maximum of ≈50 pm [see Fig. 2(d)]. The cavity length is ∼6 m. We calibrate the net gain G of a single pass through the forward and backward cavity paths independently, which takes into account all the losses but does not include the mirror reflectivity. Therefore, $G = 0$ dB corresponds to the lossless configuration, and lower values indicate a net loss. The lasing threshold is $G_L = 1/R = 3$ dB, and Poynting's threshold is $G_P = 1/\sqrt{R} = 1.5$ dB. We use a low probe power ≈10 μW to avoid any saturation effects, and we confirm the SOA linearity by injecting a probe directly into each while operating in the cavity.

We now assess the contribution of the interference term in Eq. (3). The SOA is InP-based with $n_r \approx 3.5$, while $n_i = \frac{\lambda}{2\pi d} \ln G$, where $d = 1.5$ mm is the SOA active length that provides a maximum gain of 30 dB, thus yielding $n_i/n_r \approx 10^{-4} \ll 1$. Hence, the contribution of the interference term in $\mathcal{P}_z(z)$ is indeed negligible.

4. RESULTS

We first present measurements of the power of the forward and backward waves at the cavity exits, $I_f(L)$ and $I_b(L)$, respectively,

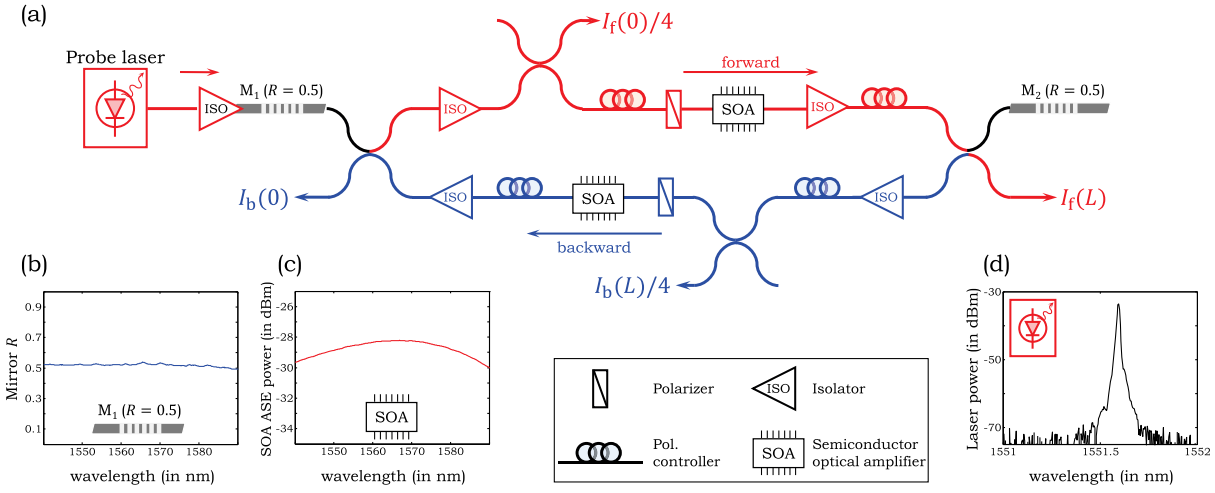

Fig. 2. (a) Schematic of the fiber-based optical setup used to observe the reversal of Poynting's vector. Lines correspond to single-mode fibers. Red and blue fibers contain solely forward or backward waves, respectively, while black fibers contain both forward and backward waves. Symmetric 3 dB fiber couplers probe the forward and backward waves at the cavity entrances $I_f(0)$ and $I_b(0)$ and exits $I_f(L)$ and $I_b(L)$, respectively. (b) Measured spectral reflectivity R of the mirrors. (c) Amplified spontaneous emission from an SOA, which serves as a measure of its spectral gain. (d) Spectrum of the probe laser.

obtained at the positions identified in Fig. 2(a) while varying G over a range extending from a passive configuration up to $G_L = 3$ dB. As predicted theoretically, at the cavity exit, $I_f(L)/I_b(L)$ is a constant when $G < G_L$, as is clear from the fixed 3 dB difference (since $R = 0.5$) on the logarithmic scale in Fig. 3(b). Consequently, $\vec{\mathcal{P}}(L)$ always points forward in the direction of the probe. We contrast these measurements with those obtained at the cavity entrance, probed at the points shown in Fig. 2(a). Here, the ratio of forward to backward propagating waves is $I_f(0)/I_b(0) = 1/(RG^2)$, which decreases with G until $G = G_P = 1.5$ dB, whereupon $I_f(0) = I_b(0)$ and thus $\vec{\mathcal{P}} = 0$ [see Fig. 3(a)]. The measurements reveal unambiguously that $I_f(0) < I_b(0)$ in the range $G_P < G < G_L$, whereupon the direction of $\vec{\mathcal{P}}$ is reversed. The measurements are in excellent agreement with our theoretical model (Supplement 1).

These results are further elucidated by measuring $I_f(z)$ and $I_b(z)$ along the cavity. The principle of the measurement is illustrated in Figs. 4(a) and 4(b). Any position z along the cavity

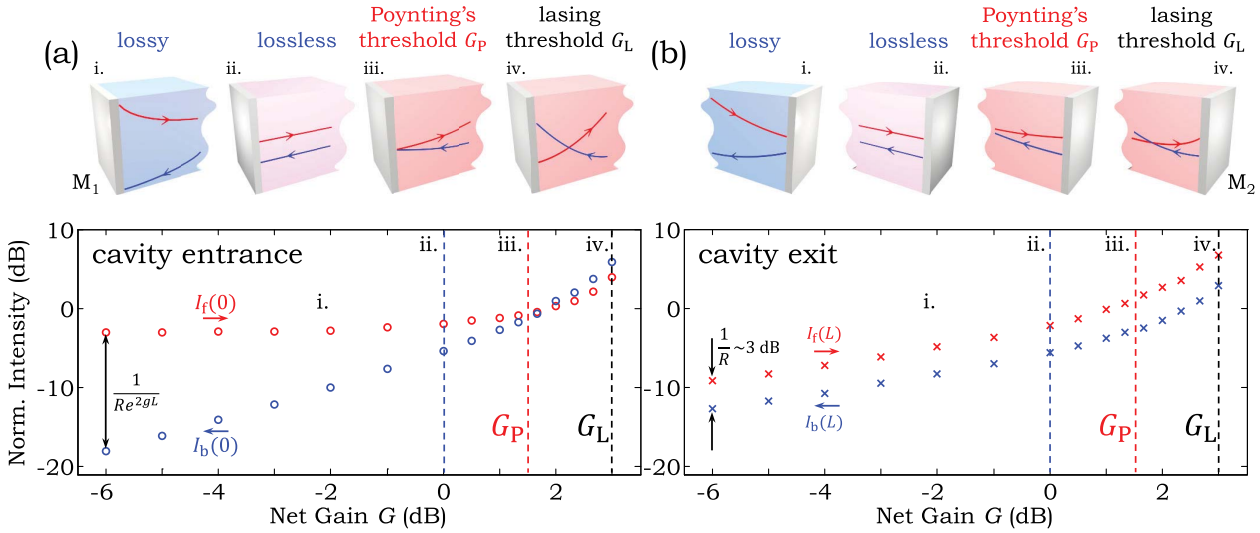

Fig. 3. Measured forward and backward power, $I_f(z)$ and $I_b(z)$, respectively. (a) Measured $I_f(0)$ and $I_b(0)$ at the cavity entrance $z = 0$ with the cavity net gain G. Schematics of the intensity distributions in the vicinity of the entrance are provided on top for the four identified values of G, (i) through (iv). (b) Measured $I_f(L)$ and $I_b(L)$ at the cavity exit $z = L$ with G. Schematics of the intensity distributions in the vicinity of the exit are shown on top for the values of G identified in (a). Here, (i) corresponds to a lossy case, (ii) to lossless, (iii) to Poynting's threshold, and (iv) to the lasing threshold.

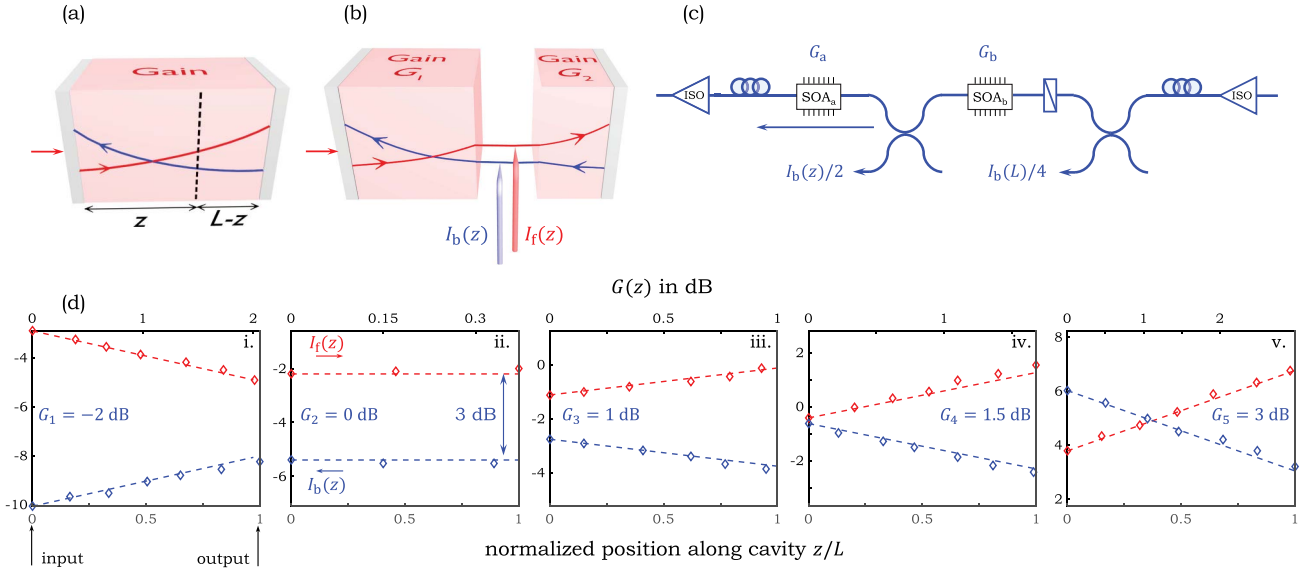

Fig. 4. Measuring $\vec{\mathcal{P}}$ along a planar cavity. (a) Schematic of the intensity distribution along a cavity above Poynting's threshold. (b) The cavity is conceptually sectioned into two segments at position z and probes obtain the values of $I_f(z)$ and $I_b(z)$. (c) Schematic of the optical setup to probe $I_f(z)$ and $I_b(z)$. We show the arm of the setup in Fig. 2(a) carrying the backward wave after replacing the SOA with two SOAs separated by a coupler to probe the signal. A similar modification is applied to the arm carrying the forward wave. (d) Measured values of $I_f(z)$ and $I_b(z)$ for selected values of net gain: $G_1 = -2$ dB (lossy cavity), $G_2 = 0$ dB (lossless cavity), $G_3 = 1$ dB (active cavity $< G_P$), $G_4 = G_P = 1.5$ dB, and $G_5 \approx 3$ dB $< G_L$ (pre-lasing). The bottom horizontal axis in each panel is the normalized cavity length z/L, while the top axis is the gain of SOA_a or $G(z)$. The dashed lines are theoretical plots that makes use of the experimental values of single-pass gain.

divides it into two segments of length z, and $L-z$ has net gains $G(z)$ and $G(L-z)$, where $G(z)G(L-z)=G$, or $G(z)+G(L-z)=G$ in logarithmic scale. This configuration is captured by replacing each SOA having gain G by a cascade of two SOAs, say $\mathrm{SOA_a}$ and $\mathrm{SOA_b}$ with gains G_a and G_b, respectively, such that $G_\mathrm{a}G_\mathrm{b}=G$. Therefore, setting $G_\mathrm{a}=G(z)$ and $G_\mathrm{b}=G(L-z)$ in both the forward and backward paths maps the point between $\mathrm{SOA_a}$ and $\mathrm{SOA_b}$ to the axial position z, and probing the forward and backward waves at this point yields $I_\mathrm{f}(z)$ and $I_\mathrm{b}(z)$, respectively, and thus $\vec{\mathcal{P}}(z)$ [see Fig. 4(c)]. By holding G fixed and increasing G_a from 1 to G while concomitantly decreasing G_b from G to 1 (maintaining a fixed overall gain), measurements at the point between $\mathrm{SOA_a}$ and $\mathrm{SOA_b}$ thus map the full range between $I_\mathrm{f}(0)$ to $I_\mathrm{f}(L)$ and $I_\mathrm{b}(0)$ to $I_\mathrm{b}(L)$.

We have measured $I_\mathrm{f}(z)$ and $I_\mathrm{b}(z)$ at five values of G [see Fig. 4(d)]. At a net loss of $G_1=-2$ dB see [Fig. 4(d-i)], $I_\mathrm{f}(z)>I_\mathrm{b}(z)$ at all z, and $\vec{\mathcal{P}}$ points forward everywhere and decays from the entrance to the exit. In the lossless configuration $G_2\approx 0$ dB, $I_\mathrm{f}(z)=I_\mathrm{b}(z)$ for all z and $\vec{\mathcal{P}}(z)$ is a constant [Fig. 4(d-ii)]. Transitioning into the active regime at $G_3=1$ dB $<G_\mathrm{P}$, the slopes of $I_\mathrm{f}(z)$ and $I_\mathrm{b}(z)$ are reversed with respect to the lossy case G_1 [see Fig. 4(d-iii)]. Nevertheless, we still have $I_\mathrm{f}(z)>I_\mathrm{b}(z)$, and $\vec{\mathcal{P}}$ points forward everywhere. At $G_4\approx G_\mathrm{P}=1.5$ dB, a null in $\vec{\mathcal{P}}$ appears at the cavity entrance [see Fig. 4(d-iv)], and at $G_5\approx 3$ dB $>G_\mathrm{P}$, this null migrates inside the cavity [see Fig. 4(d-v)] to the position z_P. In all these cases, at the exit, $I_\mathrm{f}(L)$ and $I_\mathrm{b}(L)$ differ by 3 dB, a value that is anchored by the scattering boundary conditions, as seen on the right side of each panel in Fig. 4(d). The only exception is when G approaches G_L and saturation effects lead to an increase in this difference to ≈4 dB.

5. CONTROLLABLE REVERSAL OF POYNTING'S VECTOR VIA A PASSIVE INTRA-CAVITY ELEMENT

It can be more convenient, nevertheless, to reverse $\vec{\mathcal{P}}$ by tuning a passive rather than an active element. In this section, we demonstrate that the direction of $\vec{\mathcal{P}}$ at a fixed point in a structured active cavity may be reversed *without changing its amplitude* via a passive intra-cavity element [see Fig. 5]. Here, the cavity contains an active element providing a *fixed* gain $G_\mathrm{f}>G_\mathrm{P}$ and a tunable lossy element $\mathcal{L}$, such that the net gain is $G=G_\mathrm{f}+\mathcal{L}$ (in logarithmic scale). When $\mathcal{L}=0$ dB and $G>G_\mathrm{P}$, $\vec{\mathcal{P}}$ points *backwards* at the cavity entrance [see Fig. 5(a)]. Increasing $\mathcal{L}$ reduces G, and when $G<G_\mathrm{P}$, $\vec{\mathcal{P}}$ reverses direction and points *forward* [Fig. 5(b)].

To observe this loss-induced reversal of $\vec{\mathcal{P}}$, we make use of an experimental configuration similar to that in Fig. 2(a) except for adding a lossy element. The cavity thus consists of concatenated loss (fiber variable optical attenuator) and gain (SOA) sections, we add a 99:1 fiber coupler to probe $\vec{\mathcal{P}}$ at the cavity entrance as depicted in Fig. 5(c), and care is taken to eliminate any extra reflections, so that coherent feedback is provided solely by the end mirrors $\mathrm{M_1}$ and $\mathrm{M_2}$ (Supplement 1). To increase the range of values of $\vec{\mathcal{P}}$ that may be switched without changing the amplitude, we must maximize the difference between G_P and G_L, the range over which $\vec{\mathcal{P}}$ points backward. In an asymmetric cavity where $R_1\neq R_2$, $G_\mathrm{L}/G_\mathrm{P}=1/\sqrt{R_1}$; therefore, reducing R_1 will help increase this tuning range. In our experiment, $R_1=0.04$ and $R_2=0.5$, which yields a span $\Delta G=G_\mathrm{L}-G_\mathrm{P}\approx 7$ dB. The gain is fixed throughout the experiment, and only $\mathcal{L}$ is varied. We plot in Fig. 5(d) the measured power of the forward and backward waves I_f and I_b. Two regimes are observed: $|\mathcal{L}|>|G_\mathrm{P}|$ and $0<|\mathcal{L}|<|G_\mathrm{P}|$ (in dB), in which $\vec{\mathcal{P}}$ points in the forward and backward directions, respectively. At $|\mathcal{L}|=|G_\mathrm{P}|$, $\vec{\mathcal{P}}$ is extinguished, and its magnitude increases (while pointing in different directions) when $\mathcal{L}$ is decreased or increased. We plot the magnitude $|\vec{\mathcal{P}}|=|I_\mathrm{f}-I_\mathrm{b}|$ in Fig. 5(e) while varying $\mathcal{L}$. We observe that pairs of values of $\mathcal{L}$ around Poynting's threshold, $\mathcal{L}_-$ and $\mathcal{L}_+$, produce corresponding pairs of values of $\vec{\mathcal{P}}$, $\vec{\mathcal{P}}_-$ and $\vec{\mathcal{P}}_+$, respectively, such that $|\vec{\mathcal{P}}_-|=|\vec{\mathcal{P}}_+|$ while having different signs. Therefore, by changing the added loss from $\mathcal{L}_-$ to $\mathcal{L}_+$, we switch the direction of $\vec{\mathcal{P}}$ *without* changing its amplitude.

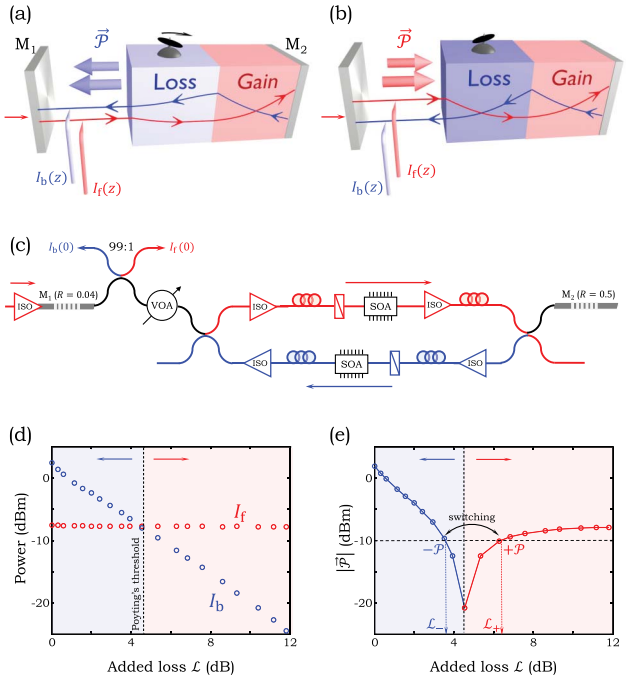

Fig. 5. Controllable reversal of Poynting's vector at a point in a structured active cavity via a passive intra-cavity element. (a) Conceptual structure of the active cavity. The forward and backward fields are probed between the mirror $\mathrm{M_1}$ and the lossy section. At low loss and high gain values, $\vec{\mathcal{P}}$ is reversed. (b) When loss in increased, $\vec{\mathcal{P}}$ points forward. (c) Schematic of the optical setup; $R_1=0.04$ and $R_2=0.5$, such that $G_\mathrm{P}=1.5$ dB and $G_\mathrm{L}=8.5$ dB. (d) Measured forward I_f and backward I_b waves at the cavity entrance while varying the loss. (e) Absolute value of $\vec{\mathcal{P}}(z)$ while varying the loss. At the values of loss $\mathcal{L}_-$ and $\mathcal{L}_+$ on different sides of Poynting's threshold, $\vec{\mathcal{P}}$ switches values from $-\mathcal{P}$ to $+\mathcal{P}$. In (d) and (e), the domains of forward and reversed $\vec{\mathcal{P}}$ are delineated by red and blue backgrounds, respectively.

Unlike traditional approaches to optical switching that rely on electro-optic effects, our approach is based on changing a lossy element without capacitive loading. In an on-chip realization, changing the loss can be achieved via current injection, which may provide certain advantages. Finally, although one may switch the direction of beam propagation by exploiting two remote sources, the process described here switches the propagation direction *locally* without needing access to the source itself.

6. DISCUSSION

We have reported, for the first time to the best of our knowledge, the observation of a predicted reversal of Poynting's vector in an active photonic cavity under scattering boundary conditions once

a critical gain value is exceeded, a value we term Poynting's threshold. We have also confirmed that the direction of power flow at a point in a cavity can be switched without changing the amplitude of Poynting's vector by modulating a lossy intra-cavity element. These results provide a new approach for molding the flow of light in non-Hermitian structures where optical gain and loss are arranged spatially in novel geometries.

The measurements were carried out in a fiber-cavity arrangement where this fundamental phenomenon can be observed unambiguously. The results are, however, of relevance to other optical realizations where the structure of the cavity or the source of optical gain are chosen differently. We note that the phenomenon we described here relies on providing coherent gain in a cavity, and thus they may also be observed in other non-Hermitian platforms for propagating waves, including acoustics [39,40] and phononics [41], and potentially even electronics [42] and magnonics [43]. Furthermore, we have considered only deterministic systems here, and it remains an open question what the impact of Poynting's threshold is in disordered active structures, especially when the disorder leads to Anderson localization [44].

Funding. Air Force Office of Scientific Research (AFOSR) (FA-9550-12-1-0148, FA9550-14-1-0037).

Acknowledgment. The authors are grateful to Amy Van Newkirk for the technical assistance, and to Guifang Li and Bin Huang for the loan of the equipment. We thank Alex Cerjan for the useful suggestions and comments, and D. N. Christodoulides, A. Miri, and R. Ahmad for the useful discussions.

See Supplement 1 for supporting content.

REFERENCES

1. A. E. Siegman, *Lasers* (University Science Books, 1986).
2. E. Desurvire, *Erbium-Doped Fiber Amplifiers: Principles and Applications* (Wiley, 1994).
3. M. G. Raymer, *The Silicon Web: Physics for the Internet Age* (Taylor & Francis, 2009).
4. A. Einstein, "Quantentheorie der strahlung," Phys. Z. **18**, 121–128 (1917).
5. L. J. Wang, A. Kuzmich, and A. Dogariu, "Gain-assisted superluminal light propagation," Nature **406**, 277–279 (2000).
6. A. Kuzmich, A. Dogariu, L. J. Wang, P. W. Milonni, and R. Y. Chiao, "Signal velocity, causality, and quantum noise in superluminal light pulse propagation," Phys. Rev. Lett. **86**, 3925–3929 (2001).
7. A. Dogariu, A. Kuzmich, H. Cao, and L. J. Wang, "Superluminal light pulse propagation via rephasing in a transparent anomalously dispersive medium," Opt. Express **8**, 344–350 (2001).
8. A. Dogariu, A. Kuzmich, and L. J. Wang, "Transparent anomalous dispersion and superluminal light pulse propagation at a negative group velocity," Phys. Rev. A **63**, 053806 (2001).
9. R. Y. Chiao and P. W. Milonni, "Fast light, slow light," Opt. Photon. News **13**(6), 26–30 (2002).
10. M. D. Stenner, D. J. Gauthier, and M. A. Neifeld, "The speed of information in a 'fast-light' optical medium," Nature **425**, 695–698 (2003).
11. M. S. Bigelow, N. N. Lepeshkin, and R. W. Boyd, "Superluminal and slow light propagation in a room-temperature solid," Science **301**, 200–202 (2003).
12. P. Palinginis, F. Sedgwick, S. Crankshaw, M. Moewe, and C. Chang-Hasnain, "Room temperature slow light in a quantum-well waveguide via coherent population oscillation," Opt. Express **13**, 9909–9915 (2005).
13. H. Su and S. L. Chuang, "Room temperature slow and fast light in a quantum-dot semiconductor amplifier," Appl. Phys. Lett. **88**, 061102 (2006).
14. B. Pesala, Z. Chen, A. V. Uskov, and C. Chang-Hasnain, "Experimental demonstration of slow and superluminal light in semiconductor optical amplifiers," Opt. Express **14**, 12968–12975 (2006).
15. B. Pesala, F. Sedgwick, A. V. Uskov, and C. Chang-Hasnain, "Electrically tunable fast light at THz bandwidth using cascaded semiconductor optical amplifiers," Opt. Express **15**, 15863–15867 (2007).
16. K. Y. Song, M. G. Herráez, and L. Thévenaz, "Observation of pulse delaying and advancement in optical fibers using stimulated Brillouin scattering," Opt. Express **13**, 82–88 (2005).
17. G. M. Gehring, A. Schweinsberg, C. Barsi, N. Kostinski, and R. W. Boyd, "Observation of backward pulse propagation through a medium with a negative group velocity," Science **312**, 895–897 (2006).
18. B. Peng, S. K. Özdemir, S. Rotter, H. Yilmaz, M. Liertzer, F. Monifi, C. M. Bender, F. Nori, and L. Yang, "Loss-induced suppression and revival of lasing," Science **346**, 328–332 (2014).
19. A. Mostafazadeh, "Spectral singularities of complex scattering potentials and infinite reflection and transmission coefficients at real energies," Phys. Rev. Lett. **102**, 220402 (2009).
20. M. Brandstetter, M. Liertzer, C. Deutsch, P. Klang, J. Schöberl, H. E. Türeci, G. Strasser, K. Unterrainer, and S. Rotter, "Reversing the pump dependence of a laser at an exceptional point," Nat. Commun. **5**, 4034 (2014).
21. R. El-Ganainy, K. G. Makris, D. N. Christodoulides, and Z. H. Musslimani, "Theory of coupled optical PT-symmetric structures," Opt. Lett. **32**, 2632–2634 (2007).
22. C. E. Rüter, K. G. Makris, R. El-Ganainy, D. N. Christodoulides, M. Segev, and D. Kip, "Observation of parity-time symmetry in optics," Nat. Phys. **6**, 192–195 (2010).
23. B. Peng, S. K. Ö. F. Lei, F. Monifi, M. Gianfreda, G. L. Long, S. Fan, F. Nori, C. M. Bender, and L. Yang, "Parity–time-symmetric whispering-gallery microcavities," Nat. Phys. **10**, 394–398 (2014).
24. L. Chang, X. Jiang, S. Hua, C. Yang, J. Wen, L. Jiang, G. Li, G. Wang, and M. Xiao, "Parity-time symmetry and variable optical isolation in active-passive-coupled microresonators," Nat. Photonics **8**, 524–529 (2014).
25. L. Feng, Z. J. Wong, R.-M. Ma, Y. Wang, and X. Zhang, "Single-mode laser by parity-time symmetry breaking," Science **346**, 972–975 (2014).
26. H. Hodaei, M.-A. Miri, M. Heinrich, D. N. Christodoulides, and M. Khajavikhan, "Parity-time-symmetric microring lasers," Science **346**, 975–978 (2014).
27. I. De Leon and P. Berini, "Amplification of long-range surface plasmons by a dipolar gain medium," Nat. Photonics **4**, 382–387 (2010).
28. M. C. Gather, K. Meerholz, N. Danz, and K. Leosson, "Net optical gain in a plasmonic waveguide embedded in a fluorescent polymer," Nat. Photonics **4**, 457–461 (2010).
29. A. A. Kolokolov, "Reflection of plane waves from an amplifying medium," J. Exp. Theor. Phys. Lett. **21**, 312–313 (1975).
30. A. V. Dorofeenko, A. A. Zyablovsky, A. A. Pukhov, A. A. Lisyansky, and A. P. Vinogradov, "Light propagation in composite materials with gain layer," Phys. Usp. **55**, 1080–1097 (2012).
31. O. Vázquez-Candanedo, J. C. Hernández-Herrejón, F. M. Izrailev, and D. N. Christodoulides, "Gain- or loss-induced localization in one-dimensional PT-symmetric tight-binding models," Phys. Rev. A **89**, 013832 (2014).
32. T. S. Mansuripur and M. Mansuripur, "Fresnel reflection from a cavity with net roundtrip gain," Appl. Phys. Lett. **104**, 121106 (2014).
33. Y.-F. Chen, P. Fischer, and F. W. Wise, "Negative refraction at optical frequencies in nonmagnetic two-component molecular media," Phys. Rev. Lett. **95**, 067402 (2005).
34. Y.-F. Chen, P. Fischer, and F. W. Wise, "Sign of the refractive index in a gain medium with negative permittivity and permeability," J. Opt. Soc. Am. B **23**, 45–50 (2006).
35. J. Skaar, "Fresnel equations and the refractive index of active media," Phys. Rev. E **73**, 026605 (2006).
36. L.-G. Wang, L. Wang, M. Al-Amri, S.-Y. Zhu, and M. S. Zubairy, "Counterintuitive dispersion violating Kramers-Kronig relations in gain slabs," Phys. Rev. Lett. **112**, 233601 (2014).
37. J. H. Poynting, "On the transfer of energy in the electromagnetic field," Philos. Trans. R. Soc. London **175**, 343–361 (1884).
38. G. P. Ortiz and W. L. Mochán, "Nonadditivity of Poynting vector within opaque media," J. Opt. Soc. Am. A **22**, 2827–2837 (2005).

39. X. Zhu, H. Ramezani, C. Shi, J. Zhu, and X. Zhang, "PT-symmetric acoustics," Phys. Rev. X **4**, 031042 (2014).
40. R. Fleury, D. Sounas, and A. Alú, "An invisible acoustic sensor based on parity-time symmetry," Nat. Commun. **6**, 5905 (2015).
41. H. Jing, X.-Y. L. S. K. Özdemir, J. Zhang, L. Yang, and F. Nori, "PT-symmetric phonon laser," Phys. Rev. Lett. **113**, 053604 (2014).
42. N. Bender, S. Factor, J. D. Bodyfelt, H. Ramezani, D. N. Christodoulides, F. M. Ellis, and T. Kottos, "Observation of asymmetric transport in structures with active nonlinearities," Phys. Rev. Lett. **110**, 234101 (2013).
43. J. M. Lee, T. Kottos, and B. Shapiro, "Macroscopic magnetic structures with balanced gain and loss," Phys. Rev. B **91**, 094416 (2015).
44. A. Basiri, Y. Bromberg, A. Yamilov, H. Cao, and T. Kottos, "Light localization induced by a random imaginary refractive index," Phys. Rev. A **90**, 043815 (2014).